24th INTERNATIONAL CONGRESS ON SOUND AND VIBRATION
23–27 July 2017, London

EFFECT OF AIRPORT SURFACE AND JET BLAST DEFLECTOR ON SUPERSONIC JETS NOISE USING RANS/ILES-METHOD

Leonid Benderskiy, Dmitriy Lyubimov, Alexandra Chestnyh

Central Institute of Aviation Motors, 111116 Moscow, Russia
email: leosun.ben@gmail.com

The RANS/ILES high resolution method was applied to calculating cold and heated supersonic jets from bi-conical nozzle. Mach number at the nozzle exit equal 1.56 which corresponds nozzle pressure ratio 4. The total temperatures at the nozzle inlet were 300K, 600K and 1050K. Calculations were carried out on structured grids containing about 4.5M-8.5M cells. A good agreement with known experimental data for the cold jet was obtained. The effect of jet heated on pressure fluctuation near the airport surface and on jet blast deflector was studied. For far-field prediction of the radiated noise, the Ffowcs-Williams & Hawkings (FWH) acoustic analogy was used. It was found that for heated jets the noise level increases at acute observation angles. The radiation pattern becomes irregular in azimuthal direction for configuration with airport surface and jet deflector. The noise level over the jets is increased due to the increase of the noise level at medium and low frequencies.

Keywords: supersonic jet, LES, jet blast deflector, jet noise

1. Introduction

The actuality of investigations of the interaction of exhaust jets with the airport surface and the jet deflector consists in the necessity to take into consideration the dynamic, thermal loads on the surfaces, jet noise and the safety zones for technique and people. This is especially important for deck aviation.

The flow in a circular jet propagating along the surface is known to be completely different from that in a free jet, i.e., significant transversal spreading of the jet along the surface is observed [1-3]. At the same time, in the cross section the size of the jet in the horizontal direction can be 8–10 times greater than the size of the jet in the vertical direction. The Reynolds-averaged Navier–Stokes (RANS) method with traditional turbulence models does not qualitatively describe this type of jet flow [4]. It was required to create an anisotropic turbulence model and introduce new defining relationships in Navier–Stokes equations for a description of such flows [1, 4]. A recent article [5], which is an extension of [1, 4], may serve as confirmation of the practical importance and attention needed to address this problem. At the same time, approach applications based on explicit resolution of the turbulent vortices allow describing the flow in a near-wall jet [6, 7].

In work [8] the interaction of jets with a jet blast deflector (JBD) on an aircraft carrier by the RANS method in the presence of wind is investigated. However, in order to obtain pressure fluctuations on deck, JBD and acoustic characteristics, the use of eddy-resolving approaches is required. Examples of such jet simulations using large-eddy simulation (LES) and RANS/LES methods are known. Thus, the interaction of an off-design supersonic jet from a bi-conical nozzle with a JBD was investigated in [7] with the aid of the monotonically implicit LES (MILES) method based on the Euler equations. The distribution of the flow and turbulence parameters in the jet and on the

surface of a JBD and the acoustic parameters in the nearby field was obtained. Simulations of off-design supersonic jet pair interactions with a jet deflector were implemented in [9] with the aid of LES and RANS/ILES. The simulations were carried out on a grid containing 4.1×10^6 cells.

The purpose of this work is investigation of flow characteristics of free and near-wall jets. Moreover, the effect of airport surface and JBD on far-field noise is studied.

2. Numerical method and simulation parameters

The method is based on Navier-Stokes equations describing the flow of a compressible gas. The transport equation for turbulence model is written in conservative form for curvilinear coordinate system. The grid lines coincide with the boundaries of computational domain, the nozzle surface. Hybrid RANS/ILES–method [10] is used to solve equations. The RANS method is used near walls and ILES is used in the rest of the computational domain. Scheme viscosity plays a role of a subgrid scale (SGS) model. The Roe method was applied to calculate non-viscous flux on cell faces. The high resolution of this method is provided by using a monotone difference scheme MP9 [11] with upwind 9th-order approximation to calculate flow parameters on cell faces. This approach has been successfully used in [12]. Diffusion fluxes are calculated on cell faces with second-order approximation by central differences. The time discretization is made with second order by implicit scheme and with integration by double- time method. The Spalart–Allmaras turbulence model is used in RANS region. The WENO–5 scheme [11] is used to calculate convective flows on cell faces in the difference analog of turbulence model equation. In LES region, the Spalart–Allmaras turbulence model is modified so that the turbulent viscosity is equated to zero. This is achieved by changing the distance in dissipative term of turbulence model equation. The modified distance $\tilde{d}$ is calculated by the formula:

$$\tilde{d} = \begin{cases} d, & d \le C_{ILES}\Delta_{MAX} \\ 0, & d > C_{ILES}\Delta_{MAX} \end{cases},$$

where d – the distance from the wall to the cell center, Δ_{MAX} – the maximum size of the cell, C_{ILES} –constant defining position of transition from RANS to ILES and equal 0.65.

This method has worked well in the calculation of sub- and supersonic jets from nozzles of different configurations [6, 10, 13-14].

For far-field prediction of the radiated noise, the Ffowcs-Williams & Hawkings (FWH) acoustic analogy was used. The free jet noise was calculated by averaging over outflow disks. This method proposed Shur et al. [15].

3. Computational meshes and simulations parameters

The position of exhaust nozzle, deck and JBD shown in Fig. 1 and corresponds [7]. The nozzle geometry is the same bi-conical (C-D) nozzle geometry as reported in [7]. Calculations are carried out on structured grids containing about 4.5M-8.5M cells. Fig. 2 shows computational grid for free jets and jets with deck and JBD.

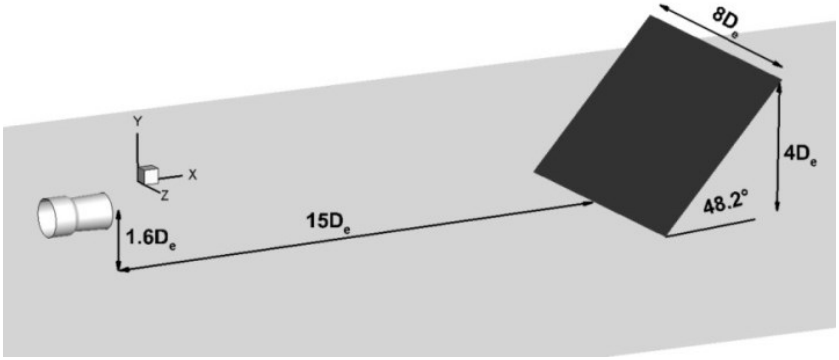

Figure 1: The position of the nozzle, deck and JBD.

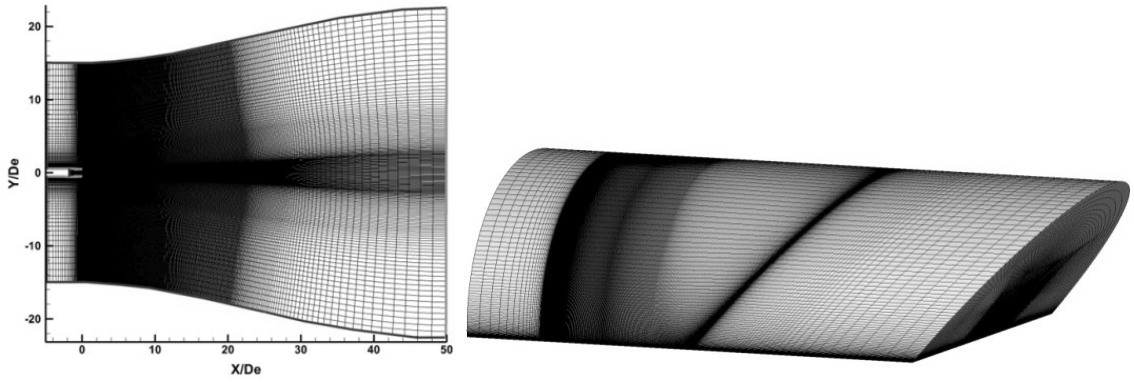

a *b*

Figure 2: *a*) Longthital section of computational grid for free jets; *b*) computational domain for jet with deck and JBD.

Total flow parameters: pressure, temperature and angle of velocity vector are set at the nozzle inlet. Boundary conditions of wall function/no-slip wall is used for nozzle, airport and JBD surface. The no-slip wall condition is applied automatically if Y^+ in the cell less 2. The far field asymptotic of the jet [10] is used for outside boundary. The static pressure is fixed for outlet boundary and other parameters have zero derivatives with respect to normal to the boundary. The computational grid step to the boundary of the computational domain increases to exclude reflections from the outlet boundary and this allows using steady boundary conditions from RANS method [10]. The modified boundary condition of the far field jet asymptotic is applied for outside boundary in case with deck and JBD. The outlet boundary is used if the velocity vector in the cell near the outside boundary is directed to outside of the computational domain.

Mach number at the nozzle exit equal M_j=1.56 which corresponds nozzle pressure ratio (NPR) 4. The total temperatures at the nozzle inlet are 300K, 600K and 1050K. Pressure and temperature in the surrounding area are P_{amb} =10^5Pa and T_{amb} =300K. Simulation parameters are show in Table 1 where U_j, T_j, M_j – parameters calculated by adiabatic relations, M_a – acoustic Mach number.

Table 1: Simulation parameters.

NPR	T_0, K	U_j, m/s	T_j, K	M_j	M_a	Re
4	300	444	202	1.56	1.28	4.148×10^6
	600	628	404		1.81	1.683×10^6
	1050	831	707		2.39	0.866×10^6

4. Simulation results

4.1 Free jet calculations

Fig. 3a shows total pressure distributions, where the experimental data are measured by using a Pitot probe. In simulation, the total pressure behind a normal shock wave evaluated by using the local Mach number since a normal shock wave is present in front of the probe when the local flow is supersonic. The radial location shown in Fig. 3a is slightly off the jet centerline by 0.1D to avoid the impact of the Mach disk. It can be seen that agreement between simulation and experiment data is very good up to X/D_e=7, after which due to coarseness of the grid simulation begin to decay earlier than in experiment. This can also be seen in Fig. 3b, which shows the axial velocity distributions in the cross sections.

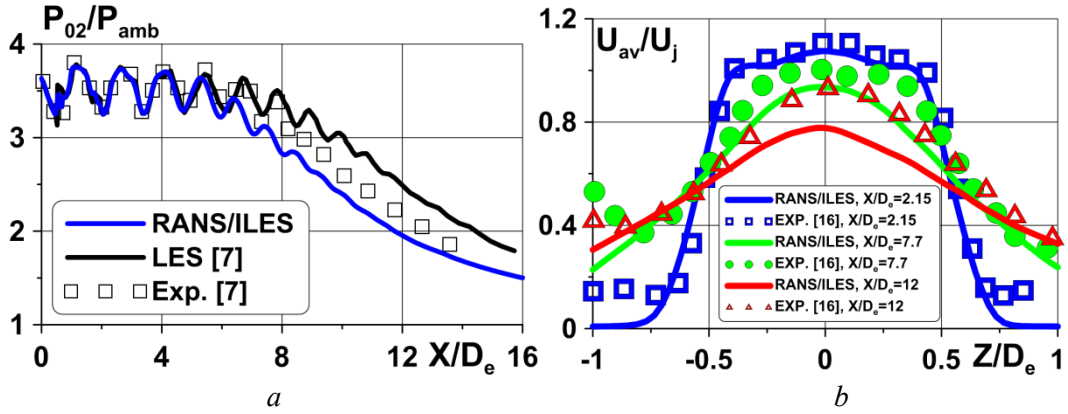

a *b*

Figure 3: *a*) The total pressure behind a normal shock wave evaluated by using the local Mach number [7]; *b*) distributions of averaged longitudinal velocity across the jet [16 AIAA 2009].

Fig. 3 shows isosurfaces of Q parameter for cold jet. The small areal of the mixing layer with toroidal vortices regular structure is observed near the nozzle exit. This is caused by "numerical transition". However, vortices are quickly destroyed and the flow becomes turbulent at approximately $1D_e$ -$2D_e$ from nozzle exit. This process is accompanied by an increased level of flow parameters fluctuations in comparison with experiment (Fig. 5a). Distributions of axial velocity fluctuation in mixed layer of jets are shown in Fig. 5a in additional, the experimental data from [17] for cold supersonic jet from nozzle with NPR=3.05 are shown.

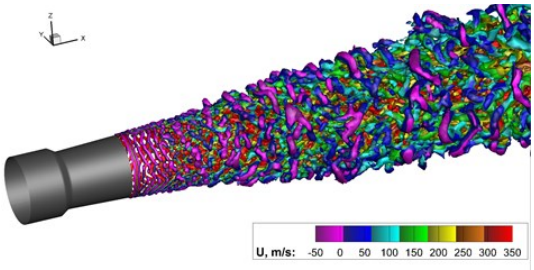

Figure 4: Isosurface of Q parameter for cold jet.

As was shown in [14], an increase in temperature of jet leads to a decrease in the length of the jet initial section (Fig. 5b) it is result of greater angle extension of the mixing layer in the hot jet. This is due to increased levels of pulsations in the mixing layer (Fig. 5a). The level of pressure fluctuation in mixing layer (Fig. 6) for hot jets is higher by approximately 50-60% up to $X/D_e=4$, after at $4<X/D_e<8$ it's higher by 20%. The pressure fluctuations of cold and hot jets become the same after $10D_e$. In additional, the experimental data of subsonic jet from [18] is shown in Fig. 6.

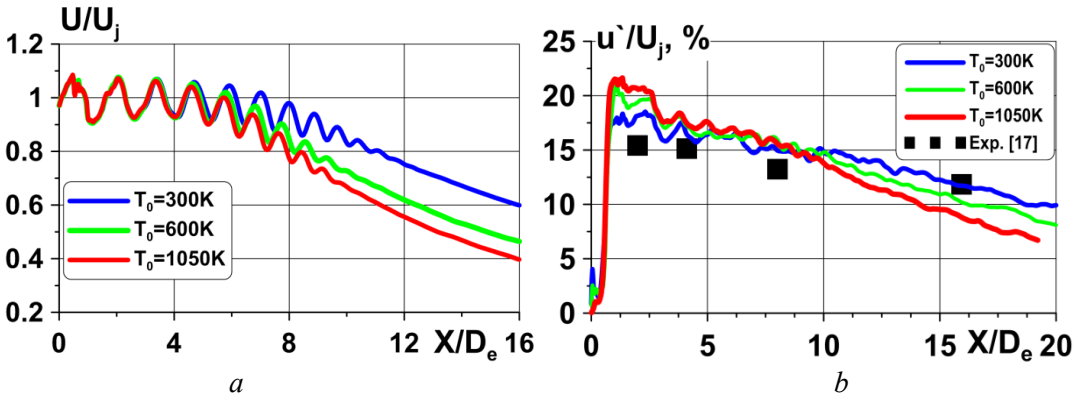

a *b*

Figure 5: *a*) Distributions of averaged longitudinal velocity along jet axis at $R/D_e=0.1$; *b*) distributions of maximum pulsations of longitudinal velocity in mixing layer.

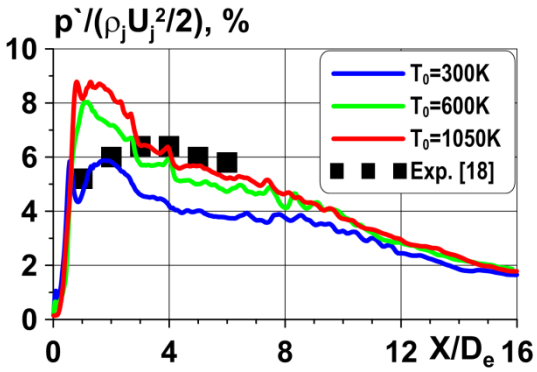

Figure 6: Distributions of maximum pulsations of static pressure in mixing layer.

The comparison of pressure fluctuation in near field of the cold jet between calculation and experimental and LES data from [7] is shown in Fig. 7a. Near field distributions are obtained from line starting from $1.5D_e$ above the nozzle exit are at angle of 7.4°. It can be seen a good agreement of noise level up to $10D_e$. The increase in the jet temperature led to an increase in jet velocity (Table 1) and in the Mach wave radiation [14], as result the noise level of hot jets is higher by 5-10 dB at $X/D_e>2$, after at $X/D_e>5$ the noise level decreases monotonically. Hot jets have pronounced maximum of noise level at $X/D_e=3$.

Fig. 7b shows overall sound pressure level (OASPL) in far field on a radius of $47D_e$. The observation angle θ is measured from the positive direction of the X-axis. The experimental and MILES simulations data from [19] are presented in Fig. 7b. It can be seen that level of cold jet noise is below the experiment approximately by 5dB. However, the effect of jet heating in this calculation are same as in [19]. The noise level increases at acute angles.

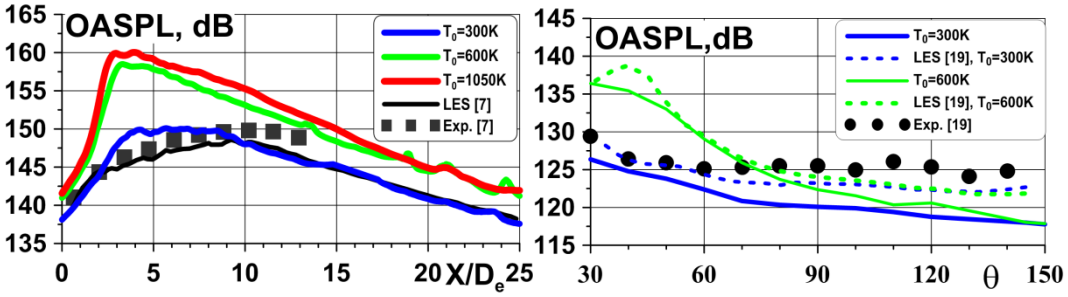

a *b*

Figure 7: Overall sound pressure level of jets noise at near field (*a*) and the far field (*b*).

4.2 Jets with the deck and JBD surfaces

The increase in jet temperature leads to an increase in pressure fluctuation at the deck. This can be seen in Fig. 8a where distributions of pressure fluctuation near the deck ($Y/D_e=-1.5$) are shown. In additions, data from MILES simulations [7] for cold jets are given. The level of pressure fluctuation of present calculation at $2.5<X/D_e<10$ are higher than in [7]. An increase in temperature of jet leads to increase in pulsations at the deck at $2.5<X/D_e<10$ by 2-10dB. This increase is due to the radiation of Mach wave, it can be see in Fig. 8b.

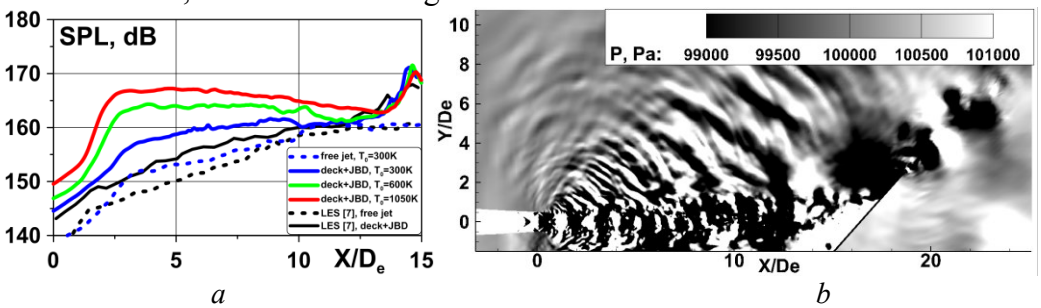

a *b*

Figure 8: *a*) Distributions of pressure fluctuations at deck ($Y/D_e=-1.5$); *b*) the field of static pressure.

The level of pressure fluctuation at JBD surface is reduced with increasing the temperature of jet (Fig. 9a). This can be explained by a decrease in the initial section of hot jets and, as a consequence, a decrease in the pressure level on JBD surface (Fig. 9b). Moreover, the pressure maximum at JBD surface locate below the jet axis, this are result of transversal spreading effect of near-wall jets [6].

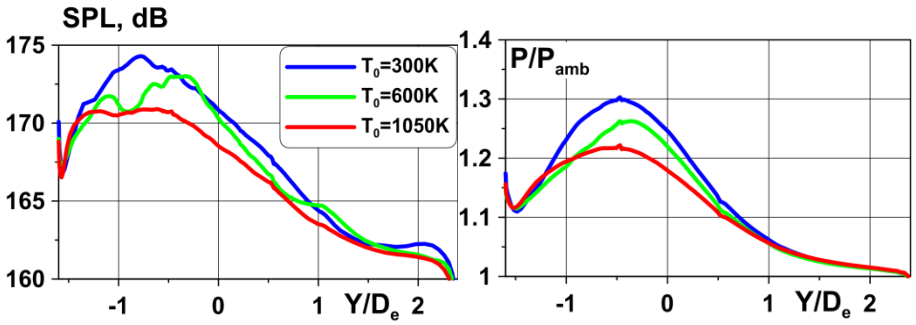

a *b*

Figure 9: Distributions of pressure fluctuations (*a*) and pressure (*b*) at centre line of JBD.

The FWH-method is used for calculation far-field noise (R/D_e=47) of near-wall jets. The Kirchhoff surface covers jet and JBD surface and is located close to them. The result of far-field calculations for cold and hot (T_0=600K) jets are shown in Fig. 10. It can be seen, that the effect of airport surface and deflector surface on the far-field noise is in irregular noise level in azimuthal direction. There is an increase in noise above the jet while the noise level from the side corresponds to noise of free jet. This can also be seen in Fig. 11, where distributions of overall sound pressure level from the side and above of jets are shown. The noise level above of cold jet is increased by 5dB and the local maximum are located at observation angle 90°-100°. The maximum difference for hot jets is found at 110° and equal approximately 7dB.

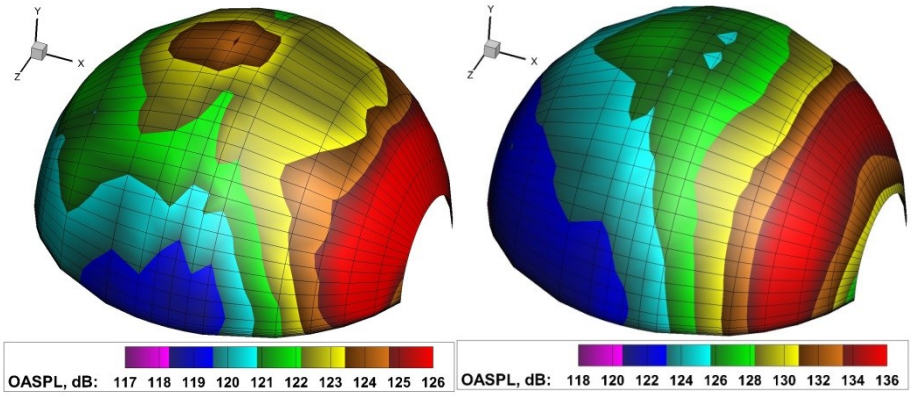

a *b*

Figure 10: Overall sound pressure level of jets noise at the far field on sphere R/D_e=47 for cold jet (*a*) and jet with T_0=600K (*b*).

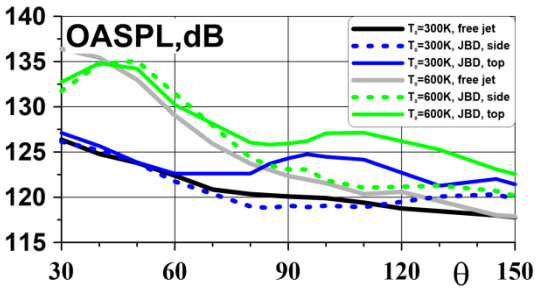

Figure 11: Overall sound pressure level of jets noise at the far field.

Fig. 12 shows one-third octave spectra of jet noise for different observation angle. It is most likely that an insufficient grid resolution near the Kirchhoff surface for case with deck and JBD

resulted in a noise difference on high frequency (S_h>2) between free jets and jets with JBD. It can be seen that there is a decrease noise of hot (T_0=600K) near-wall jet by 5-7dB after S_h=0.2 at observation angle 30° (Fig. 12a). This leads to decrease overall noise level by 4 dB (Fig. 11). The influence of the deck and JBD surfaces on the spectra of observation angles 90° and 110° above jets is manifested in significant increase in noise at low frequencies (S_h<0.5) by 10dB and an increase in noise level at spectrum maximum (0.5<Sh<2) by 2-7dB. This is the reason for an increase in the OASPL (Fig. 11) at observation angles greater than 90°. The noise spectra of observation angles 90° and 110° from the side of jets does not changed significantly.

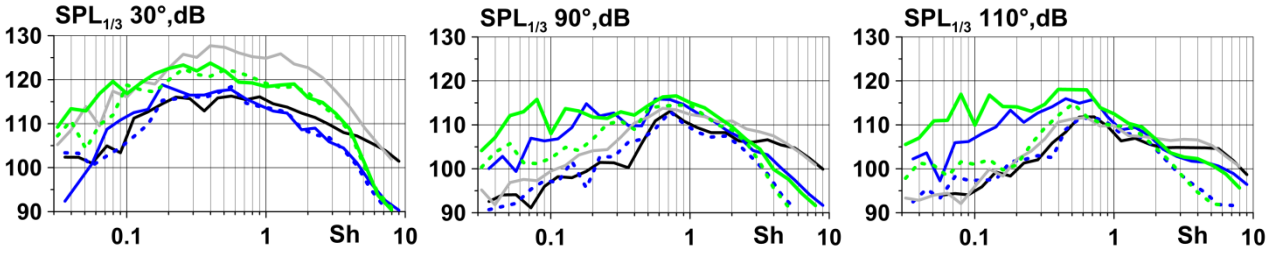

Figure 12: 1/3-octave noise spectra of jets for observation angle of 30°, 90° and 110°. The legend as in Fig. 11.

5. Summary

Calculations of supersonic jet flow from bi-conical nozzle were carried out with help high-resolution RANS/ILES method. The good agreement by flow parameters of cold free jet was obtain between simulations and experiment. It was demonstrate that the increase the jet temperature leads to reduce the initial section of jet.

The effect of jet temperature on pressure fluctuation at airport and JBD surfaces was obtained. There is the increase of pressure fluctuation at the deck and a reduce pulsations level on the deflector with an increase of jet temperature. The increase of pulsations level at deck is due to the radiation of Mach wave.

The far-field noise calculation for near-wall jets showed strong irregular noise pattern in azimuthal direction.

The noise level from the side corresponds to noise of free jet while there is an increase in noise above jets by 5-7dB for observation angle above 90°. This increase is due to the rise of the noise level at medium and low frequencies.

This work was supported by RFBR (grant number 15-08-01996 A).

REFERENCES

1 Khritov, K.M., Lyubimov, D.A., Maslov, V.P., Mineev, B.I., Secundov, A.N., Birch, S.F. Three-dimensional wall Jets: Experiment, Theory and Application, *AIAA P*, **2002-732**, (2002).

2 Agelin-Chaab, M., Tachie, M.F. Characteristics and structure of turbulent 3D offset jets, *International Journal of Heat and Fluid Flow,* **32**, 608-620, (2011).

3 Davis, M.R., Winarto, H. Jet diffusion from a circular nozzle above a solid plane, *J. Fluid Mech.,* **101(1)**, 201-221, (1980).

4 Berch, S. F., Lebedev, A. B., Lyubimov, D. A., Sekundov, A. N. Modeling of Three-Dimensional Turbulent Jet and Boundary-Layer Flows, *Fluid Dynamics*, **36(5)**, 712-725, (2001).

5 Ishiko, K., Hasimoto, A., Matsuo, Y., Yoshizawa, A., Nishiyama, Y., Nakamura, Y. One-Equation Extended Nonlinear Turbulence Modeling in Predicting Three-Dimensional Wall Jets, *Journal of Aircraft,* **51(2)**, 584-595, (2014).

6 Bendersky, L. A., Lyubimov, D. A., Potekhina, I. V., Fedorenko, A. E. Application of the high-resolution RANS/ILES technology for flow simulation and the nearby acoustic field of near-wall jets and mixing layers, *TsAGI Science Journal*, **47(2)**, 159–183, (2016).

7 Liu, J., Corrigan, A., Kailasanath, K., Ramammurti, R., Heeb, N., Munday, D., Gutmark, E., Impact of Deck and Jet Blast Deflector on the Flow and Acoustic Properties of Imperfectly Expanded Supersonic Jets, *AIAA P.*, **2013-323**, (2013).

8 Kuizhi, Y., Liangliang, C., Hu, L., Yunliang, W. Analysis of jet blast impact of embarked aircraft on deck takeoff zone, *Aerospace Science and Technology*, **45**, 60-66, (2015).

9 Erwin, J.P., Sinha, N., Rodebaugh, G.P. Noise predictions of a hot twin-jet impinging on a jet blast deflector, *AIAA P.*, **2013-324**, (2013).

10 Lyubimov, D.A. Development and application of a high-resolution technique for Jet flow computation using large eddy simulation, *High Temperature*, **50(3)**, 420-436, (2012).

11 Suresh, A., Huynh H.T. Accurate Monotonicity-Preserving Schemes with Runge–Kutta Time Stepping, *J. Comput. Phys.*, **136(1)**, 83–99, (1997).

12 Grinstein, F.F., Margolin, L.G., Rider, W.J. *Implicit Large Eddy Simulation: Computing Turbulent Fluid Dynamics*, Cambridge University Press, (2007).

13 Bendersky, L. A., Lyubimov, D. A. High-resolution RANS/ILES method for complex turbulent jets, *TsAGI Science Journal*, **45(3-4)**, 215-236, (2014).

14 Benderskiy, L.A., Lyubimov, D.A. Investigation of flow parameters and noise of subsonic and supersonic jets using RANS/ILES high resolution method, *Proceedings of the 29-th Congress of the International Council of the Aeronautical Sciences*, St. Petersburg, Russia, 7-12 September, (2014).

15 Shur, M. L., Spalart, P. R., Strelets, M. Kh., Noise prediction for increasingly complex jets. Part I: Methods and tests, *International Journal of Aeroacoustics*, **4(3&4)**, 213-246, (2005).

16 Liu, J., Kailasanath, K., Ramamurti, R., Munday, D., Gutmark, E., Lohner, R. Large-Eddy Simulations of a Supersonic Jet and Its Near-Field Acoustic Properties, *AIAA Journal*, **47(8)**, 1849-1864, (2009)

17 Lau, J.C. Effects of exit Mach number and temperature on mean-flow and turbulence characteristics in round jets, *J. Fluid Mech.*, **105**, 193-218, (1981).

18 Jones, B.G., Adrian, R.J., Nithianandan, C.K., Plachon, H.P. Spectra of Turbulent Static Pressure Fluctuations in Jet Mixing Layers, *AIAA J.*, **17(5)**, 449, (1979).

19 Liu, J., Corrigan, A.T., Kailasanath, K., Heeb, N.S., Munday, D.E., Gutmark, E.J. Computational Study of Shock-Associated Noise Characteristics Using LES, *AIAA P.*, **2013-2199**, (2013).